JOURNAL OF SPACECRAFT AND ROCKETS
Vol. 47, No. 4, July–August 2010

Dynamic Fluid Interface Experiments Aboard the International Space Station: Model Benchmarking Dataset

Ryan M. Jenson* and Mark M. Weislogel†
Portland State University, Portland, Oregon 97207
and
Jörg Klatte‡ and Michael E. Dreyer§
University of Bremen, 28359 Bremen, Germany

DOI: 10.2514/1.47343

This paper introduces a video database reduced from the handheld capillary flow contact line experiments completed aboard the International Space Station during expeditions 9–16, August 2004–November 2007. The simple fluid interface experiments quantify the uncertain impact of the boundary condition at the contact line: the region where liquid, gas, and solid meet. This region controls many significant static and dynamic characteristics of the large length scale capillary phenomena critical to multiphase fluids management systems aboard spacecraft. Differences in fluid behavior of nearly identical static interfaces to nearly identical perturbations are attributed primarily to differences in fluid physics in the vicinity of the contact line. Free and pinned contact lines, large and small contact angles, and linear and nonlinear perturbations are tested for several manually imparted perturbation types (i.e., axial, slosh, and other modes) to right circular cylinders. The video and sample digitized datasets are made publicly available for model benchmarking. As a demonstration of the utility of the database, and in parallel with the experimental effort, blind numerical predictions of the dynamic interface response to the experimentally applied input perturbations are offered as an example of current capabilities to predict such phenomena. The agreement and lack of agreement between the experiments and numerics is a guide to improve or verify current analytical methods to predict such phenomena critical to practical spacecraft fluid systems design.

I. Introduction

CAPILLARY flows and phenomena are critical to many important fluids management systems in low-gravity environments such as fuels/cryogen storage systems, thermal control systems (e.g., vapor/liquid separation), life support systems (e.g., water recycling), and other materials processing in the liquid state. Under microgravity conditions, the impact of dominant capillary forces must be well understood if such large mission-critical systems are to perform predictably. To enhance such understanding, the capillary flow experiments (CFE) aboard the International Space Station (ISS) were designed as a collection of quantitative fundamental and applied capillary phenomena experiments conducted using handheld hardware. The experiments address certain aspects of interface dynamics and stability, critical geometric wetting, and three-dimensional wicking including passive phase separations. The general aim of the broader CFE effort is to provide results of incremental value to the low-gravity fluid systems design community that cannot be readily obtained in ground-based tests. Results from the CFE contact line (CL) experiments are reported here. Further CFE details may be found elsewhere [1–4].

Presented as Paper 2008-816 at the 46th AIAA Aerospace Sciences Meeting and Exhibit, Reno, Nevada, 7–10 January 2008; received 24 September 2009; revision received 23 March 2010; accepted for publication 26 March 2010.

*M.S. Candidate, Department of Mechanical Engineering, P.O. Box 751-ME.

†Professor, Department of Mechanical Engineering, P.O. Box 751-ME. Member AIAA.

‡Ph.D. Candidate, Research Scientist, Center for Applied Space Technology and Microgravity, Am Fallturm.

§Senior Scientist, Professor, Center for Applied Space Technology and Microgravity.

II. Motivation and Overview

Knowledge of the curvature of a capillary dominated fluid interface is central to understanding both the static and dynamic behavior of the interface and in turn the locations of the fluid phases it divides. For example, the liquid center of mass (i.e., location), natural frequency, damping, and stability all depend critically on the base state static or dynamic curvature of the interface. Unfortunately, such curvature in turn depends critically on the particular wetting conditions at the contact line: the absence of an accurate physical description of which remains a potentially serious design impediment. Over the past 40 years numerous authors have reviewed the fertile research field of static and dynamic wetting and the pivotal role of the moving contact line boundary condition [5–10]. Despite the literature being replete with insightful studies the seemingly limitless variety of wetting surfaces and scenarios tend to overwhelm the designer who is perhaps more interested in a boundary condition that merely produces design specific results than in a boundary condition that is actually physically correct. The establishment of the latter may still be decades away despite significant recent achievements [10]. In the meantime, the low-gravity fluids systems designer is faced with computing large-scale interfacial phenomena (large length$\sim \mathcal{O}$(m), large mass $\sim \mathcal{O}$(tons)) potentially critically dependent on an ill-defined microscale boundary condition at the moving contact line. Some argue that this shortcoming is of little consequence and that present methods are adequate [11]. The present experimental study seeks to report data that might be used to put such issues to rest from an applications perspective.

The CL experiments provide a low-gravity dataset useful in comparing extremes in dynamic contact line conditions. More important, it serves as a dataset suitable for model benchmarking. The dynamic interface experiments employ partially filled right circular cylinders for which a large ground-based low-gravity experiment history is established [12–16], the most recent works of which represent the state of the art. The present work extends the database by providing hundreds of dynamic interface events to initially quiescent low-gravity surfaces, each event requiring from 5 to 30 s of low-gravity time to fully decay. These data may be used by design

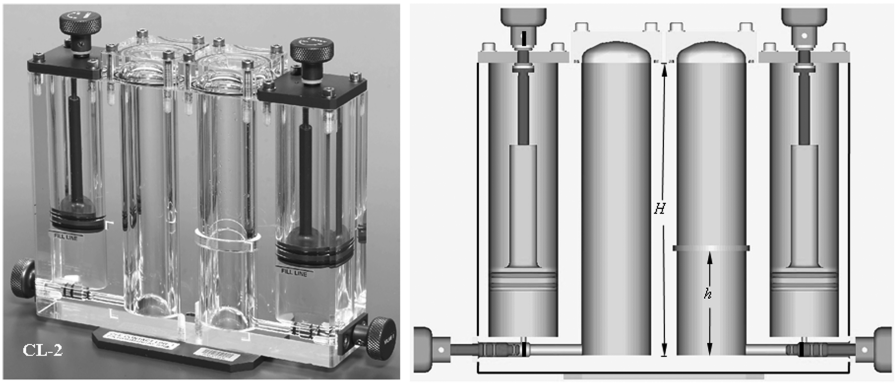

a) Image **b) Solid model with dimensions**

Fig. 1 CL vessel.

engineers, theoreticians, and numerical analysts to benchmark current and future models.

In this paper a description of the CL hardware is provided followed by the general experiment operating procedure. A list of the tests performed with pertinent statistics is provided, but the complete video database is the contribution of this work and is made publicly available on the internet.[¶] A description of our data reduction and organization methods is reviewed and employed here for presentation of example data. As a demonstration of the utility of the database a representative subset of the flight data is then compared with blind numerical predictions made using only the empirically determined perturbations. The short term impact of such comparisons is discussed in conclusion.

III. Description of CFE-CL Hardware

The two CL ISS flight experiment units were envisioned with the principle design drivers of safety, a short delivery schedule, small mass (less than 2 kg each), small volume (less than 2 L each), no electrical power requirements, and minimal to no crew training requirements, while providing a direct means to quantitatively determine the extremes in dynamic fluid interface behavior expected from free or pinned contact line conditions. A photograph of the CFE-CL-2 flight unit is provided in Fig. 1 along with a solid model of the design with dimensions noted. The two units are identical in all respects save wetting properties, fluid volume, and pinning lip location. The main body is machined from a single piece of cast acrylic and fitted with aluminum pistons and stainless steel piston drive screws. The right circular cylindrical test chambers have flat bases but elliptical acrylic lids.

Each unit is secured to an aluminum base plate with a single slotted hole that is used for attachment to the ISS maintenance work area (MWA) via a captive fastener allowing for as much as 40 mm lateral motion or adjustment. (Note that the MWA provides a rigid surface on which to perform maintenance tasks on ISS. The MWA consists of a folding aluminum tabletop and two detachable arms. The arms attach to the seat track, providing the table with two solid connection points.) Turning a knob connected to a drive screw displaces the piston. The knob diameter and screw pitch are selected so that a slow and stable manual fill process is assured. The double O-ring sealed reservoirs, charged at atmospheric pressure ($\approx P_{\text{atm}}$), hold the 2 cst silicone oil test liquid and employ pistons to dispense the liquid into the respective test sections. Thus, the test chambers are somewhat pressurized ($\approx 1.3 P_{\text{atm}}$) when the liquid is fully deployed. The design meets a single level of containment requirement for a zero-hazard test liquid enabling the experiments to be performed by any crew member in the open ISS laboratories.

A requirement of the experiment is to fill the cylinders to identical levels with the same liquid establishing nearly identical interface configurations. The only difference between the interfaces in the different cylinders is that one of the contact lines is pinned at a pinning edge created by a groove machined into the cylinder walls (cylinder at right in Fig. 1 with dimensions noted in Table 1). Because the cylinders are closely and rigidly coupled, any manually imparted disturbance to the vessel produces nearly identical disturbances to both smooth and pinning cylinders. Such disturbances are not highly controlled or repeatable, but they are highly quantifiable and disturbance inputs and interface responses (i.e., frequency and damping rates) are quantified herein to at best ± 90 μm and at worst ± 125 μm from the video data (720×480 pixel charge-coupled device at 30 fps). Our comparisons of the data for a variety of disturbances identify the physical bounds that can be expected for the assumptions of free and pinned contact line conditions. Idealizations of these limiting conditions are often imposed by numerical methods used to predict such phenomena and can lead to significant departures from observations [17–19]. As demonstrated herein, the quantified disturbances and resulting interface responses provide an adequate dataset to benchmark theoretical and numerical models.

The CL-1 unit tests a partially wetting liquid with a contact angle of $\approx 50^\circ$ while the CL-2 unit tests a perfectly wetting (spreading), zero contact angle liquid. The selection of a 38.1 mm cylinder diameter is constrained by an ISS safety requirement for maximum fluid volume. The cylinder diameter and fluid depth are sized to be as large as possible within this constraint to access uniquely low-gravity inertial-capillary regimes. The liquid volume and height of the pinning lip are also selected such that the liquid depth from the centerline of the low-gravity menisci to the cylinder base is the same for both CL-1 and CL-2 at $h = 31.75$ mm (depth/radius of 1.67). These and other container specifics are summarized in Table 1.

Certain wetting barriers are applied to the containers to enhance control during the experiment operations. The surface coating conditions vary between CL-1 and CL-2. The entire interior surface of CL-1 is rinse coated with FC-724, a transparent fluoropolymer surface coating manufactured by the 3M Corporation. CL-2 is intended to be a perfectly wetting experiment thus only for the pinning cylinder the interior surfaces above the pinning lip are coated, including the groove making up the pinning edge. The discontinuous wetting boundary established across the pinning lip in CL-2 creates a passive means of returning the fluid from above the pinning edge to below it via a favorable wetting discontinuity. The lid of the smooth cylinder is also coated. All other surfaces of CL-2 are uncoated and exhibit perfect wetting, $\theta = 0^\circ$. The equilibrium contact angle for the silicone oil on the FC-724 surface is determined by measuring advancing and receding contact angles using a tilted FC-724 coated glass capillary tube [20]. These values are listed in Table 1. The equilibrium angle is computed [21] to be $48.7 \pm 2^\circ$, but is frequently referred to as 50° in reference to CL-1. Contact angle values identified during the flight experiments confirm these values despite the test units being stored for approximately two years before the flight tests.

[¶]Data available online at http://cfe.pdx.edu [retrieved 10 October 2008].

Table 1 Physical properties and important dimensions

Properties	Values
Physical dimensions	
Cylinder diameter	38.10 ± 0.05 mm
Cylinder height H	146.0 ± 0.1 mm
Pinning lip height	7.6 ± 0.1 mm
Pinning lip diameter	43.7 ± 0.1 mm
Elliptical lids	——
Major diameter	38.1 ± 0.1 mm
Minor diameter	20.0 ± 0.1 mm
Acrylic refractive index, N_D	1.491
CL-1 specifics	$\theta = 50°$ (nominal)
Base to pinning lip, h	36.9 ± 0.1 mm
Max fluid volume	39.04 ml
CL-2 specifics	$\theta = 0°$
Base to pinning lip, h	50.80 ± 0.1 mm
Max fluid volume	43.44 ml
Fluid properties (ISS temp 25°C)	
Fluid	Silicone oil
Viscosity, ν	2 cst $\pm$ 2%
Density, ρ	872 ± 5 kg/m^3
Surface tension, σ	0.0187 N/m $\pm$ 5%
Refractive index, N_D	1.390
CL-1 specifics	$\theta = 50°$ (nominal)
Advancing, θ_{adv}	$52.2 \pm 2°$
Receding, θ_{rec}	$47.3 \pm 2°$
Equilibrium, θ_{eq}	$48.7 \pm 2°$

IV. Procedures, Performance, and Sample Data

The CL experiments require up to 3 h for setup, complete nominal operations, and tear down. Continuous video coverage is not possible due to loss of contact with the ISS during its approximately 90 min orbit. Nonetheless, during each performance, ample real-time video and audio downlink were available to provide the ground-based science team with a feeling similar to conducting the experiments in person. Following the experiments, the astronauts downlink continuous video data temporarily recorded on the onboard video system (VTR). All real-time and postexperiment downlink video data was stored on the ground for preliminary analysis despite its decreased resolution (due to compression) and reduced frame rate (as low as 8 frame/s). It was used to help specify subsequent tests and in some cases provides original data. The flight tapes (40 min ISS DVCam videotapes) have all been returned to Earth and now serve as the source for all nominal resolution data reduction. Additionally, significant science events were recorded by downlink video during periods when the ISS camcorder was not operating. These data certainly compliment the flight tapes and are analyzed to extents possible.

A typical experiment setup is shown in Fig. 2. The ISS camcorder is secured to the ISS rail, not the MWA, and aligned by eye normal to the front face of the CL vessel. Any lack of orthogonality can be corrected through image processing on the ground. A sheet of paper serves as a diffuse backlight screen. Sample static and dynamic images of the fluid interfaces taken from the flight video tapes are shown in Fig. 3. As previously stated, because the two cylinders are rigidly and closely connected any disturbance imparted to the vessel is nearly identical to both fluid interfaces and significant differences in fluid response are largely a consequence of the different conditions at the contact line. As a case in point, simultaneous meniscus centerline location z_{cl} and 1/2 radius radial location ($\equiv r_{1/2}$) histories are digitized from the video data and presented in Fig. 4 for both smooth and pinning cylinders in response to axial and slosh (push) disturbances, respectively (refer to Fig. 3 for notation). The disturbances to the containers (insets) and the general data reduction methods will be discussed shortly. It is clear by even casual inspection of Fig. 4 that the fluid response depends on the contact line boundary condition. (Note that for large amplitude axial disturbances, the centerline location of the interface is often obscured from view and thus experimental data can only be collected in such cases after the disturbance has ceased, i.e., Fig. 4a.)

The general experimental procedures are as follows: After observations of the liquid interface in response to the natural ISS background g-environment (typically $\sim 10^{-5} g_o$) the astronaut manually imparts several disturbance types to quiescent low-gravity surfaces. (Note that the background g-level of the ISS did not produce detectable disturbances to the interface.) The disturbance types pertinent to CL include tap, axial, push, slide, multislide, and swirl, and are briefly described here. The axial and push modes are the focus of this paper, but this lists reports that other disturbance types were pursued as well, since most are also included in the video database.

Solitary taps (impulses) of gradually increased magnitude are imparted to the rigidly mounted test vessel beginning with the pad of a finger and ending with light raps with a knuckle. Low-amplitude high-frequency damped oscillations of the interfaces are observed that can only be marginally resolved from the flight tapes.

Axial-mode disturbances are imparted to a CL vessel fixed to the MWA by displacing and releasing the MWA table itself, much like a diver does to a diving board (refer to inset plot in Fig. 4a). The MWA thus serves as a highly damped cantilever imparting axial disturbances of easily variable amplitude to the cylinders. Linear and nonlinear axial perturbations are imparted in this manner with amplitudes increasing to the point of droplet ejection or jet formation (ejected droplet diameters $\approx$15 mm).

The push disturbance is an impulselike disturbance leading to damped slosh-mode oscillations of the interface (see inset plot in Fig. 4b). The screw fastening the CL unit to the MWA is loosened for this disturbance such that the vessel may slide left to right in the field of view yet remain flush with the MWA surface. The push is imparted by finger across the field of view, gradually increasing the disturbance amplitude from linear to nonlinear regimes.

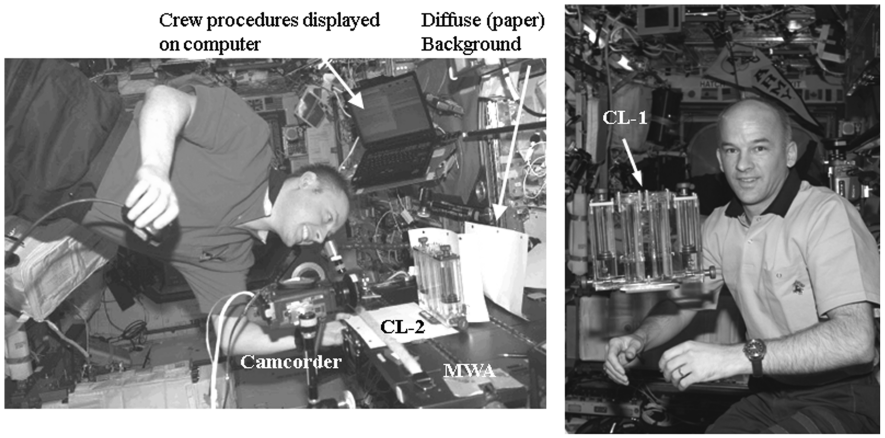

a) Michael Fincke b) Jeffrey Williams

Fig. 2 Astronauts on ISS during CFE-CL experiments.

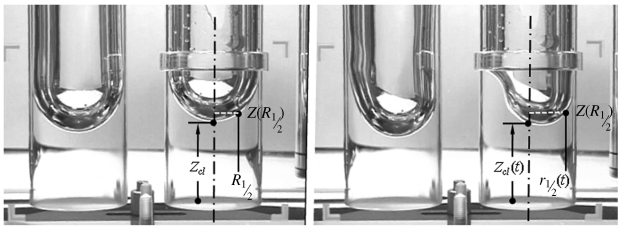

a) Quiescent initial conditions b) Dynamic nonlinear response

Fig. 3 Smooth and pinned interfaces for CL-2. Note that *Z* and *R* are defined for the quiescent interface.

Similar to the push, the slide disturbance is a single full-period lateral oscillation completed within the field of view at the approximate natural frequency of the interfaces. The peak-to-peak amplitude of the full period disturbances is varied while the frequency of the slide is held approximately constant.

A multislide disturbance is defined as a multiple $(2, 3, 4+)$ period lateral oscillation completed within the field of view at the approximate natural frequency of the interfaces. The peak-to-peak amplitude of the full period disturbances is varied while the frequency of the multislide is held approximately constant.

The swirl disturbance is defined as a swirling slosh-mode induced to the fluid using an elliptical or circular sliding motion of the CL vessel in the plane of the MWA. The fastener is removed for these tests. The swirl disturbance diameter is approximately 30 to 40 mm with swirl periods increasing incrementally from one to five. The larger-amplitude swirl disturbances yield centrifugal force-dominated vortical flows.

Care is taken to postpone disturbances that depin the pinning cylinder interface. A wait time is specified between each disturbance for all visible interface oscillations to decay, typically 5 to 60 s. In general, destabilized interfaces can be reconfigured at will using a manual astronaut-defined centrifugal method, but at the cost of up to 10 min of crew time.

Because the disturbances are imparted manually, the possibility of precisely repeating a given disturbance is unlikely. Nonetheless, three-dimensional image analyses can be used to quantify the frequency and amplitude of each disturbance such that all disturbance inputs are known with sufficient accuracy. The tap, axial, push, slide and multislide disturbances result in damped axial or slosh-type oscillations that are readily compared for both smooth and pinning cylinders. For brevity, only sample results for the axial and push disturbances are presented herein.

V. Brief Summary of Science and Extrascience Results

Hundreds of individual datasets for CFE-CL were recorded towards the nominal science objectives. Many additional tests were also conducted for what is considered extrascience. Extrascience runs were conducted by the astronauts during their offduty hours. A chronology of experimental efforts by the astronauts is outlined below.

The first performance of CL-2 (Fincke), nominal science run, included the successful completion of all science objectives with the additional demonstration of a manual centrifugal technique (a twirling astronaut) to reset the experiment for certain repeat runs, identified a controlled method to impart axial-mode disturbances using MWA, and completed noteworthy additional science involving droplet ejections, drop-wall impacts and rebounds, hourglass interface formation in the smooth cylinder, and axial annular film pumping during lateral disturbances.

The second performance of CL-2 (Fincke), extrascience, included repeat push and slide tests, as well as new data using the axial-mode. Noteworthy additional science included push disturbance viscous damping as a function of liquid depth.

During the third performance of CL-2 (McArthur), extrascience, a different manual centrifuge method (a repetitive radial arm motion with periodic hand strike) was demonstrated to fully clear the pinning lip of liquid allowing for the indefinite repetition of the experiments. Repeat push, slide, and axial-mode (camera accidentally mounted to MWA negates several axial-mode tests) tests were performed along with noteworthy additional science of more droplet/jet ejections, drop-wall impacts, and rebounds.

During the fourth performance of CL-2 (Williams), extrascience, the manual centrifugal pinning lip clearing method was perfected and repeat push, slide, and axial-mode (camera-mounted ISS rail) tests were completed. Noteworthy additional science included significant droplet/jet ejections and manifold droplet-wall and free surface impacts and rebound events.

During the first performance of CL-1 (Williams), nominal science run, all science objectives were completed with additional depth effect tests performed.

During the second performance of CL-1, (Whitson), extrascience, large amplitude axial-mode pinned oscillations and destabilizations were studied. Unfortunately, larger accelerations than could be imparted by hand were required to clear the pinning edge of liquid and the experiment was terminated prematurely.

In addition to the now considered foundational axial-mode tests, which were conceived on orbit and originally considered as extrascience, a significant number of extrascience measurements and observations are made of dynamic interfacial phenomena of both general and practical interest. Some of these tests are highly complementary to the CFE-CL investigation, such as liquid depth effects to axial and slosh-type disturbances. Others tests, such as the behavior of ejected drops and their impacts with solid and fluid surfaces, have nothing to do with the original CL science objectives. Several such extrascience tests are reported elsewhere, all of which yield quantitative data. A more detailed summary of extrascience CFE-CL data is provided in [4].

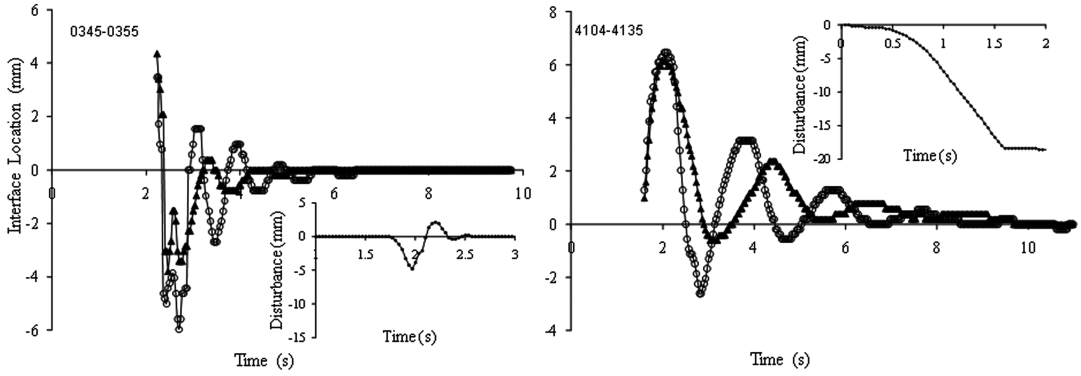

a) Axial disturbance, $z_{cl}(t)$ b) Push disturbance, $r_{1/2}(t)$

Fig. 4 Superposition of simultaneous smooth (triangles) and pinning (open circles) cylinder dynamic interface responses. Input disturbance data shown in insets.

VI. Data Reduction, Analysis, and Organization

The CL data collection, reduction, and organization effort required over three years. The video sources consist of real-time downlink video and VTR dump video in addition to the actual ISS camcorder flight video tapes recently returned to Earth. The purpose of the data reduction effort is to provide general statistics of the tests performed, but more importantly, to make the experimental data more accessible to subsequent researchers and numerical model developers. Approximately 90% of such data employs the highest resolution onboard video tape data. At present, over 350 individual tests have been digitized including approximately 30 extrascience events. These include approximately 54 axial (A), 36 push (P), 2 slide (S), and 14 multislide (MS) disturbances for CL-1 and approximately 41 axial, 70 push, 93 slide, and 47 multislide disturbances for CL-2. A database has been developed that links each dataset (i.e., test number, test container, disturbance type, etc.) to the digitized data tables and plots of both the input disturbance and fluid response, as well as to the original image (i.e., video file) of the event. The CFE-CL video library alone is all that is necessary for one to benchmark a particular model. All details associated with the data reduction such as image analysis protocol, coordinate origins, scale factors, optical corrections, etc., are provided in the database, which is publicly available via university server (see footnote [¶]). Several download options are available including single events, content based on disturbance type (axial, slide, push, etc.), and a complete download per experiment type (CL-1, 850 MB; CL-2, 875 MB), the latter which includes the reduced data, original video, and a summary page. The database is the primary contribution of this paper and a variety of analyses can be conducted with these information sources.

VII. Sample Blind Numerical Predictions, Comparisons, and Discussion

Because the CL dataset provides a unique opportunity to test and eventually benchmark analytical predictions, as a facile demonstration of this process and the use of the CL data toward this end, blind numerical computations are conducted of select CL datasets using the empirically applied input disturbances. This exercise serves as an authentic open loop test of current capabilities to predict sensitive phenomena rarely verified by experimental data. The numerical demonstration here is not closed in that following the predictions the numerical method is not revisited to improve agreement with the experiments as would be the case in a typical benchmark process. Nonetheless, the degree of success of the present computations is not without practical implications. A brief overview of the numerical approach selected is provided here before comparisons of specific cases.

Several numerical methods have been applied to the general problem of large length scale capillary reorientation in right circular cylinders, including at least FIDAP software (Ansys, Inc., e.g., see [20]), Flow3D software (Flow Science, Inc., e.g., see [3]), and now OpenFoam (OpenCFD, Ltd.). The latter is employed in this analysis with the OpenFoam CFD toolbox, an object-oriented C++ open source library supplied with a complete set of preconfigured solvers and utilities. The incompressible two-phase Navier–Stokes solver interFoam, which tracks the interface using a volume-of-fluid method, is chosen for the model. All computations in this work are conducted on three commercial computers, i.e., single core 2.8 GHz, 32-bit, Intel Pentium 4 processors, with 1 GB RAM. The majority of the somewhat optimized computations typically run overnight or longer requiring approximately 2 h of computation time for each second of actual experiment or flow time (herein denoted for example as 2 hr/s).

In keeping with the blind analysis concept, only fluid properties, test cell dimensions, and precise disturbance information are provided to the numerical analyst. Sample empirically determined disturbance data is presented in Fig. 5 in the form of CL container position as a function of time. The data is first smoothed (Fig. 5a) and then differentiated twice to obtain the time dependent acceleration (Fig. 5b). A time-varying body force vector is then implemented in the interFoam solver to model the input disturbance. It will be shown that the smoothing algorithm applied to the input disturbance has negligible impact on the fluid response predicted.

Because the computations are blind, grid resolution, refinement, and optimization must be decided without the aid of the experimental results themselves. Thus, low-resolution precalculations are performed to assess the general fluid response to the experimentally provided disturbance in order to select the appropriate mesh and mesh refinements in regions of highest velocity gradients and in particular near the contact line. This exercise also provides an estimate of the experiment flow time. The precalculations employ 10,000 cells and require approximately 30 min each. Subsequent to such calculations, a grid-type is chosen for the most optimal computations. In this case the computational mesh is modeled by 100,000 hexaeders, using the implemented block-mesh grid generator. As shown in Fig. 6, there are local refinements near the free surface and the contact line. Without the advantage of fluid specific contact line data available a priori a constant contact angle is specified as the moving contact line boundary condition. Though there are certainly physical grounds in support of this boundary condition at nanoscales [8], its application at the milliscale of the numerical domain might raise some suspicion. Nonetheless, this boundary condition has proven successful in previous studies [15,16] and naturally accommodates the pinned contact line condition at an abrupt edge.

Further computational details are presented in Fig. 7 for CL-2 ($\theta = 0°$) in response to an axial disturbance. Figure 7a demonstrates that the numerical results for the interface response are essentially independent of the Loess smoothing interpolation function of the

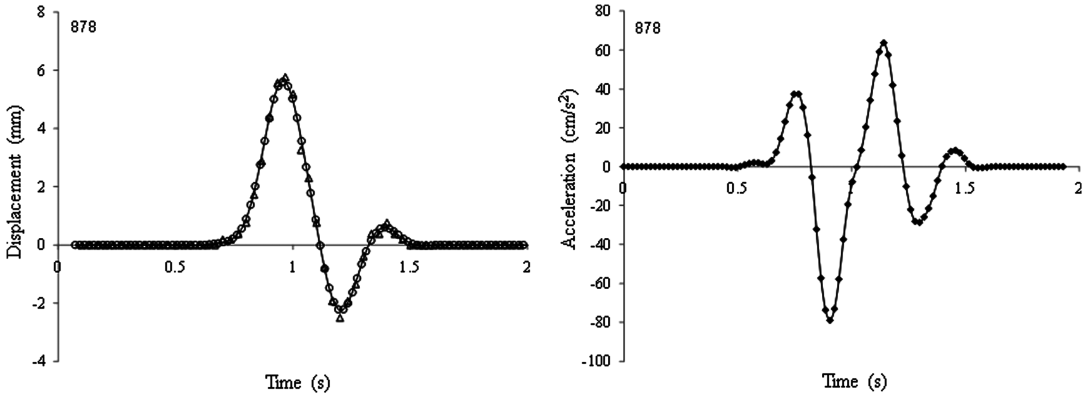

a) Raw (open triangles) and Loess smoothed (open circles/line) displacement data

b) Disturbance acceleration history using smoothed displacement data in a)

Fig. 5 Displacement and acceleration data for typical axial disturbance for axial disturbance to CL-2 ($\theta = 0°$), assumed identical for both smooth and pinning cylinders.

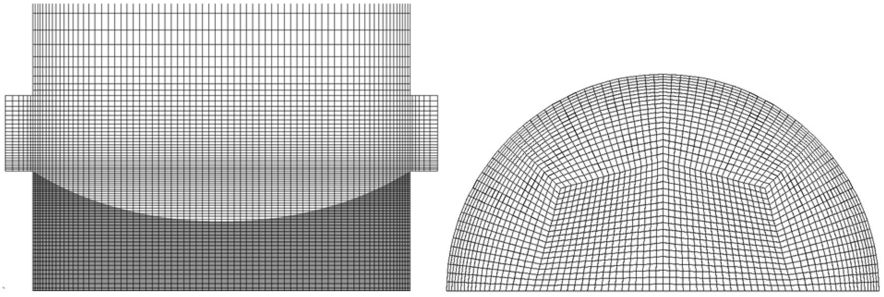

a) Extruded layers with refinements at pinning edge

b) Cross-sectional half domain using quadrangles, Blockmesh

Fig. 6 Assessment of the numerical approach for interface response to a typical axial disturbance to CL-2 ($\theta = 0°$).

empirically derived input disturbance. The highest smoothing function was employed for all calculations. To determine the dependence of the solutions on the chosen computational grid, an additional cross-sectional pattern was examined. The second mesh is generated automatically with the open source grid generator Gmsh V2.0.8 (Geuzaine and Remacle) using a mixed grid with prisms and hexaeders and again local refinements at the contact line. The comparison is presented in Fig. 7b. It is clear from observations of the figure that the results converge as the resolution increases. However, the computational time required for the structured grid in Fig. 6 (block-mesh-fine) is 50% that of the automatically generated grid for equivalent accuracy. The structured grid is selected for all computations on these grounds. Finally, in Fig. 7c a grid resolution study demonstrates the general convergence of the solution with increased mesh refinement and that the 100,000 cell model at 2.14 hr/s ($L = 0.63$ mm) computational time is a practical choice over the 200,000 cell model at 8.08 hr/s ($L = 0.5$ mm), especially considering that certain events require greater than 15 s of flow time. The experimental CL-2 data for this test case is provided postcomputations for reference. It should be noted that the increased refinement leads to increased agreement with the data and that even low grid densities produce potentially adequate results for design purposes (i.e., 10,000 cells with $L = 1.37$ mm yields 0.15 hr/s computational time, while 30,000 cells with $L = 0.94$ mm yields 0.57 hr/s). The 1/2-domain is solved for the slosh-mode disturbances while the 1/4-domain is solved for axial modes. It is also important to note that all numerical computations for CL-1 using $\theta = 50°$ are carried out, despite the experimentally determined value of $\theta = 48.7 \pm 2°$ with noted hysteresis, Table 1.

Sample computations are presented in Figs. 8–11 for CL-1 ($\theta = 50°$) and CL-2 ($\theta = 0°$), for axial and push disturbances, and for both smooth and pinning cylinders. The open circles are the numerical predictions and the triangles are the experimental data. The disturbance profiles are presented as insets on each plot. The interface centerline values are scaled equally for ease in comparisons. The axial disturbance comparisons overlay the interface (meniscus) centerline history $z_{cl}(t)$ with that determined for the experiments. The push disturbance comparisons overlay the radial location of the optical 1/2-radius location of the static interface profile $r_{1/2}(t)$ as identified in Fig. 3b. In other words, the $r_{1/2}(0) = R/2$ location identifies the z-axis location of the interface that is tracked in the radial (lateral) dimension in time. Because of an index of refraction mismatch between the liquid and the acrylic container a ray trace correction is employed to shift the location of the numerically determined $r_{1/2}$ such that both numerical and experimental locations are coincident. Note that experiment measurements for push disturbances are made at $r = 9.52$ mm ($=0.5R$, where $R = 19.05$ mm), but must be corrected for optical distortion such that the true radial location of such measurements is $r = 9.87$ mm. The numerical value for $r_{1/2}$ uses the latter location for the comparisons.

Several key characteristics of the dynamic interface response are compiled in Table 2, where Fig. 12 provides nomenclature for the table quantities. Included are experimental and numerical values for linear natural frequency f, linear damping rate ζ, number of periods N used in determining the damping rate and frequency, and maximum nonlinear and linear experimental vs numerical amplitude ratios λ. The amplitude ratios provide a measure of the accuracy of the maximum computed amplitude of the interface oscillations compared with those observed in the experiment. The linear regime is defined by oscillation amplitudes less than $\sim 0.1R$ (approximately 2 mm). The damping rate ζ is defined as the best fit to the decay function $\exp[-\zeta t]$ in the linear regime. Amplitude A_{exp} provides an assessment of the nonlinearity of the perturbation as the absolute peak-to-peak amplitude of the first experimentally determined oscillation in millimeters. Note that values for $A_{exp} < 4$ mm in Table 2 yield interface oscillations that are considered linear.

As can be observed from the comparisons by inspection, in general, the blind numerical results are in surprisingly favorable agreement with experiment. Experimental frequencies between 0.45 and 2.55 Hz, damping rates between 0.15 and 1.11 s^{-1}, and maximum interface deflection ratios between 0.08 and 5.65 are

Table 2 Comparisons of select experimental and numerical results from Figs. 8–11

	f_{exp}, Hz (±1%)	f_{num}, Hz (±1%)	ζ_{exp}, s^{-1} (±%err.)	ζ_{num}, s^{-1} (±%err.)	N_{exp}	N_{num}	A_{exp}, mm	λ_{nl}	λ_l
			CL-1: $\theta = 50°$						
Axial									
Pinned	2.55	2.50	0.67 (10)	0.30 (5)	20	20	4.50	5.65	3.58
Smooth	2.50	1.66	0.52 (10)	0.50 (5)	20	15	3.10	——	0.65
Push									
Pinned	1.31	1.17	0.15 (10)	0.15 (5)	16	14	16.20	1.85	2.68
Smooth	1.24	0.54	0.17 (10)	0.27 (5)	10	5	8.50	0.08	0.79
			CL-2: $\theta = 0°$						
Axial									
Pinned	1.13	1.11	1.11 (4)	1.04 (3)	3	5	9.80	1.45	0.60
Smooth	1.05	1.07	1.00 (-)	1.04 (-)	2	2	5.50	0.84	——
Push									
Pinned	0.53	0.45	0.62 (4)	0.30 (3)	4	5	10.00	0.85	0.65
Smooth	0.48	0.48	0.70 (8)	0.73 (2)	3	3	7.40	1.60	4.10

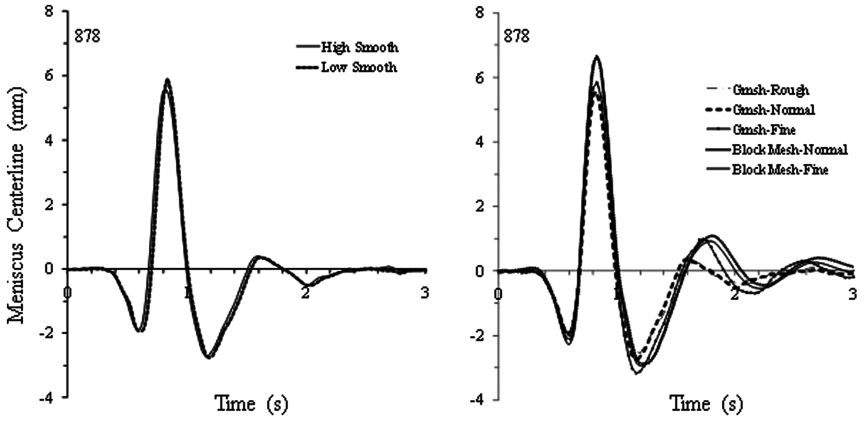

a) Impact of the smoothing (cf. fig. 5) is negligible b) Solutions for two mesh generators at various refinements

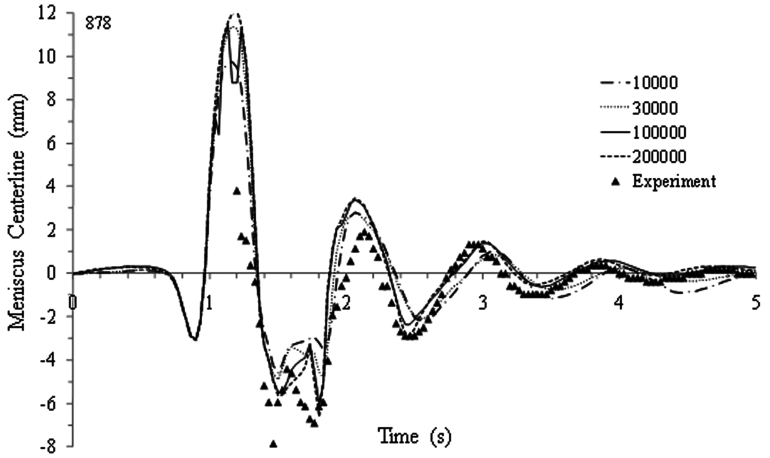

c) Convergence of solution with increased grids

Fig. 7 Computational grid for the push simulation (CL-1, $\theta = 50°$, pinning cylinder).

listed. Not listed in the table are dynamic Bond numbers ($Bo = \rho a R^2/\sigma$, where a is the local acceleration, ρ if the liquid density, and σ is the surface tension) which vary between 1.9 and 13.2 for the tests presented. Note that characteristic frequencies are on the order $f \sim (\sigma/\rho R^3)^{1/2} \approx 1.8$ Hz and characteristic settling times for free contact line conditions are on the order of 4.9 s for CL-1 ($\theta = 50°$) and 3.7 s for CL-2 ($\theta = 0°$) [13]. Several routine observations from both the experiments and numerical comparisons are provided here.

Firstly, for a given cylinder the axial disturbance, natural frequency is approximately twice that of the first subharmonic push disturbance (slosh) frequency. For a given disturbance, the CL-1 (partial wetting, $\theta = 50°$) natural frequency is approximately 2.5 times that of CL-2 (perfect wetting, $\theta = 0°$). For the push disturbance the pinning cylinder natural frequency is higher than that of the smooth cylinder.

In general, agreement between the numerics and experiment is most favorable for the perfectly wetting condition (CL-2, $\theta = 0°$), Figs. 9 and 11. This is in part due to the highly damped nature of the resulting flows, which naturally reduces the sensitivity of the flow to the boundary condition applied at the contact line: smooth and pinning cylinders respond similarly. For perfect wetting (CL-2, $\theta = 0°$) the axial disturbance is well-predicted as might be expected from previous numerical experience [15,16] but the push disturbance

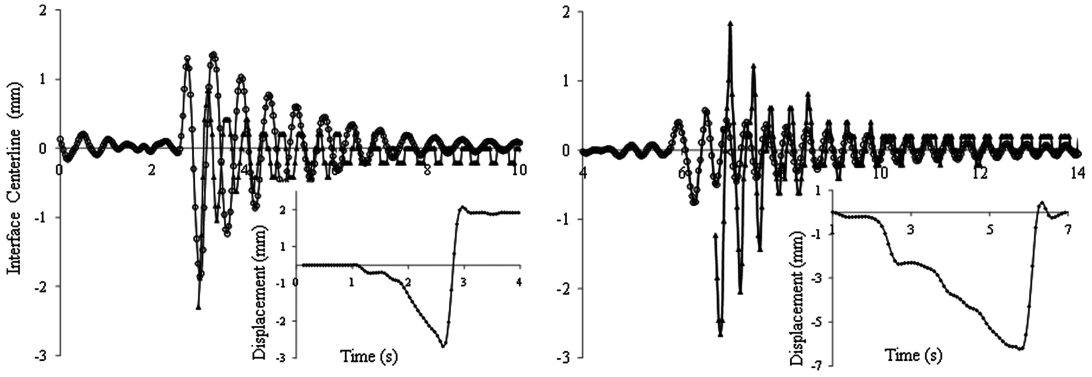

a) Smooth b) Pinned

Fig. 8 Interface centerline history $z_{cl}(t)$ for axial-mode disturbance for CL-1 ($\theta = 50°$). Open circles are numerical values, triangles are experimental.

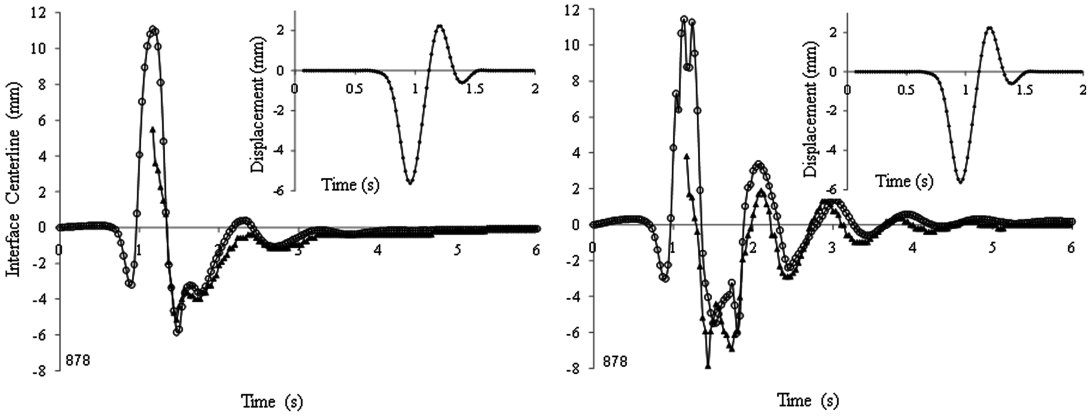

a) Smooth b) Pinned

Fig. 9 Interface centerline histories $z_{c1}(t)$ for axial-mode disturbance for CL-2 ($\theta = 0°$): note identical disturbance (inset).

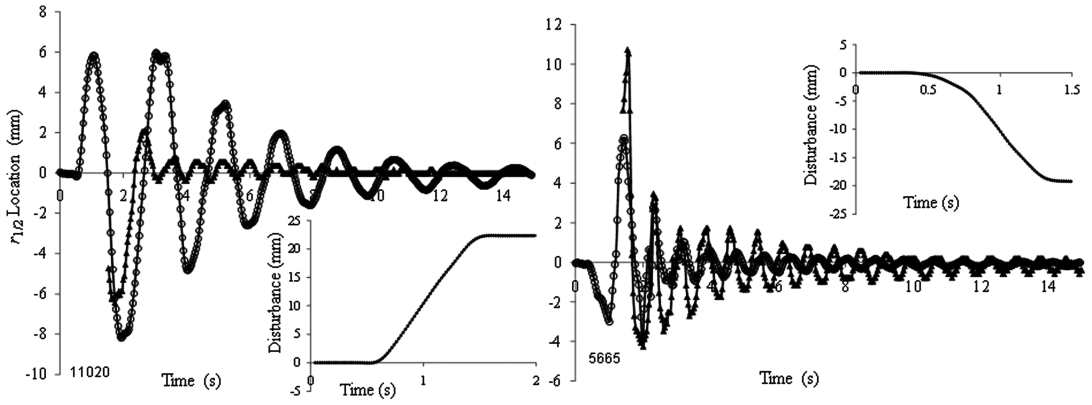

a) Smooth b) Pinned

Fig. 10 Radial $r_{1/2}(t)$ interface location history for push disturbance for CL-1 ($\theta = 50°$).

for the pinned case is replicated less favorably with ∼10% discrepancies in natural frequency with underpredictions of damping rates by a factor of two (see Fig. 11b). Errors in the smooth case are restricted to the amplitude predictions. The most quantitative agreement in terms of oscillation amplitude, frequency, and decay rate is achieved for the perfectly wetting push disturbance (Fig. 11a) followed closely by axial disturbance and the perfectly wetting condition (CL-2) for both smooth and pinning cylinders, Fig. 9. Discrepancies arise most noticeable for the partial wetting case (CL-1, $\theta = 50°$), where despite the poorer agreement the pinning cylinder results fair better than those of the smooth cylinder. The increased inaccuracy is primarily due to the choice of contact line boundary condition, and is readily observed over the manifold weakly damped oscillations, Fig. 8. The axial disturbance leads to 33% underpredictions in amplitude and frequency for the smooth case and 2.2-fold overpredictions of damping rate for the pinned case. Note that an n-fold overprediction in the damping rate implies an n-fold underprediction in overall characteristic axial settling time. The least quantitative comparisons arise for the partial wetting case ($\theta = 50°$, CL-1) and push disturbance where an up to ∼10-fold overprediction in interface amplitude is experienced in the smooth cylinder (around 4 s in Fig. 10). In effect, the numerical results remain nonlinear for an extended period. In addition, the linear frequency is underpredicted by ∼60%. The pinned condition of the contact line is likely more

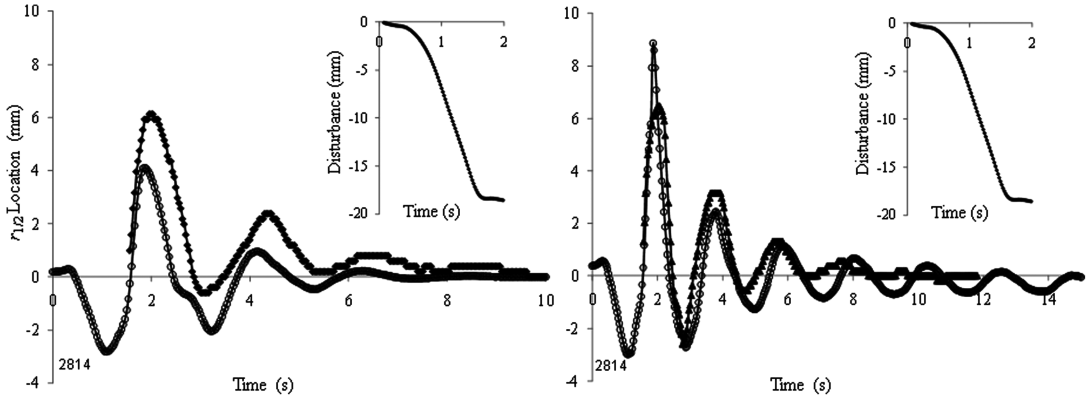

a) Smooth b) Pinned

Fig. 11 Radial $r_{1/2}$ interface location history for push disturbance for CL-2 ($\theta = 0°$); note identical disturbance (insets).

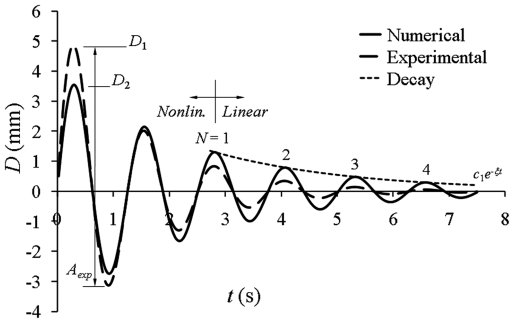

Fig. 12 Sample decay providing nomenclature for Table 2 quantities.

appropriate as the boundary condition for the smooth cylinder in this case and would largely account for the frequency error. The partial wetting conditions demand a model incorporating advancing and receding contact angle data such as employed in [15]. In addition, interfaces pinned at abrupt edges can experience mixed pinned and free contact line behavior for large oscillations where the interface pins in the advancing state, but depins to a free condition at the extremes of the receding state. To close the model benchmark exercise one would adapt the contact line boundary condition until acceptable agreement is achieved for both axial and push modes for both free and pinned states. This improved model could then be used to predict other more complex disturbance types where CFE-CL or other low-gravity data are available, before serving as a robust tool for such complex interface dynamics aboard spacecraft.

Several practical conclusions may be drawn for these low-mode oscillation comparisons:

1) The current blind OpenFoam model performs surprisingly well to predict the large length scale capillary phenomena for highly wetting systems with a simple static contact angle boundary condition at the contact line.

2) The model may be successfully prepared via precalculations improving the likelihood of accurate and efficient computations for design and analysis.

3) Efforts to further improve the general numerical approach should focus on the boundary conditions necessary to specify partial wetting systems with contact angle hysteresis and for mixed pinned and smooth contact line situations where interfaces encounter abrupt edges.

The latter step was not taken in this work. Spacecraft fluid systems employing partially wetting fluids (i.e., water processing systems) will likely require parametric studies for the various conditions that can arise at the contact line represented in their extreme cases by perfect slip and perfectly pinned conditions.

VIII. Additional Science

While performing the CL experiments, extrascience was conducted as a supplement to the primary science objectives. Extrascience was not always intentional, but managed to produce noteworthy observations (i.e., data). The topics listed here are intended to provide an idea of additional science that may be gleaned from the CL experiments and can be investigated further using the online database. Examples include: axial-mode jetting and subsequent droplet ejections, rebound impacts, satellite droplet ejections following partially wetting drop-wall coalescence events, dynamic contact line stability investigating drop ejections and depinning, axial-mode frequencies as a broader function of contact angle, and axial annular fluid film pumping attributed to laterally imparted disturbances. Additional descriptions are contained in [4,22].

IX. CFE-CL Database Description

In the CFE database (see footnote ¶), each experiment event is accompanied by an MPEG-1 video and corresponding data sheet describing physical parameters, tracking methods, raw data, and preliminary results. data sheets are designed such that one can repeat the data reduction exactly if desired, or develop one's own method. The primary components of the database are the summary page, MPEG-1 video, and individual data sheets corresponding to each video event. Each data sheet and corresponding video can be accessed through the summary page. In addition, the summary page contains select statistics and results obtained from the individual data sheets. For our digitization, the original MPEG-1 video is read into the freeware program VirtualDub software (V1.8.1) and saved as an uncompressed AVI. The converted video is then digitized using the freeware program Spotlight-8 (NASA GRC software). At any point the data can be modified by the user. For the complete database along with video, updates, and current information, see footnote ¶.

X. Conclusions

The handheld CFE-CL experiments recently completed aboard ISS serve as a general database with which to evaluate and benchmark numerical models used to design and analyze large length scale capillary systems common on spacecraft. The CL experiments demonstrate pinned and free contact line boundary conditions for a variety of disturbances to quiescent low-gravity interfaces including axial, slosh, and other modes. Axial and slosh (i.e., push) disturbances are reported herein. A sample of digitized flight test results is presented as indicative of what is made publicly available on permanent archive including a video library with digitized disturbance and interface response data (see footnote ¶). A selection of the flight tests are predicted in-the-blind using CFD. The encouraging preliminary agreement improves confidence in current numerical methods to predict capillary dynamics in highly wetting scenarios (i.e., tankage for fuels and cryogens). The comparisons also imply that more work is required to establish similar confidence in partial wetting scenarios that depend more substantially on the moving contact line boundary condition (i.e., water processing systems). The steps to further adapt the numerical method and so complete the benchmark exercise were not pursued in this investigation.

Acknowledgments

This work is supported in part by NASA through contract NNC05AA29A and by the Federal Ministry of Economy and Technology through the German Aerospace Center under grant number 50 WM 0535. The authors are deeply indebted to astronauts Michael Fincke, William McArthur, Jeffrey Williams, and Peggy Whitson for successful capillary-flow-experiment contact-line space experiments performed on International Space Station (ISS), expeditions 9, 12, 13, and 16, respectively. In several instances the experiments were performed during the crew's personal time as voluntary science. Special thanks are due to Charles Bunnell of Zin Technologies for an enduring commitment to the engineering success of capillary flow experiments. The authors are also grateful for the project science and management support of R. Green and D. Bohman of NASA John H. Glenn Research Center at Lewis Field (GRC), the engineering support of Debra Lyden of Zin Technologies, and to the NASA ISS cadre members at GRC, NASA Marshall Space Flight Center, and NASA Johnson Space Center, for assistance during the missions and in meeting the demanding development schedule. We happily acknowledge the terrestrial experimental support of Oregon High School summer students through the merit-based Apprenticeships in Science and Engineering Program at Portland State University: D. Hahs, E. Garbacek, D. Masulis, B. Pederson, P. Bhide, K. Yamauchi, J. Green, A. Vasquez, S. Shin, C. Lee., R. Kimball, A. Nicolaysen, E. Kittlaus, W. Chan, and M. Justel.

References

[1] Weislogel, M. M., Collicott, S. H., Gotti, D. J., Bunnell, C. T., Kurta, C. E., and Golliher, E., "The Capillary Flow Experiments: Handheld Fluids Experiments for the International Space Station," 42nd AIAA Aerospace Sciences Meeting and Exhibit, AIAA Paper 2004-1148, Reno, NV, 5–8 Jan. 2004.

[2] Weislogel, M. M., Bunnell, C. T., Kurta, C. E., Golliher, E. L., Green, R. D., and Hickman, J. M., "Preliminary Results from the Capillary Flow Experiment on ISS: the Moving Contact Line Boundary Condition," 43rd AIAA Aerospace Sciences Meeting and Exhibit, AIAA Paper 2005-1439, Reno, NV, 10–13 Jan. 2005.

[3] Weislogel, M., Jenson, R., Klatte, J., and Dreyer, M., "Interim Results from the Capillary Flow Experiment Aboard ISS: The Moving Contact Line Boundary Condition," 45th AIAA Aerospace Sciences Meeting and Exhibit, AIAA Paper 2007-747, Reno, NV, 8–11 Jan. 2007.

[4] Jenson, R. M., Weislogel, M. M., Tavan, N. T., Chen, Y., Semerjian, B., Bunnell, C. T., et al., "The Capillary Flow Experiments Aboard the International Space Station: Increments 9–15, August 2004–December 2007," NASA CR 2009-215586, May 2009.

[5] Dussan, V. E. B., "On the Spreading of Liquids on Solid Surface Static and Dynamic Contact Lines," *Annual Review of Fluid Mechanics*, Vol. 11, 1979, pp. 371–400. doi:10.1146/annurev.fl.11.010179.002103

[6] Davis, S. H., "Contact Line Problems in Fluid Mechanics," *Journal of Applied Mechanics*, Vol. 50, Dec. 1983, pp. 977–982. doi:10.1115/1.3167210

[7] Kistler, S. F., *Hydrodynamics of Wetting, in Wettability*, edited by J. C. Berg, Vol. 49, Surfactant Science Series, Marcel Dekker, New York, 1993, pp. 311–430.

[8] Koplik, J., and Banavar, J. R., "Continuum Deductions from Molecular Hydrodynamics," *Annual Review of Fluid Mechanics*, Vol. 27, 1995, pp. 257–292. doi:10.1146/annurev.fl.27.010195.001353

[9] Ramé, E., *Moving Contact Line Problem: State of the Contact Angle Boundary Condition, Encyclopedia of Surface and Colloid Science*, Marcel Dekker, New York, 2002, pp. 3602–3618.

[10] Ralston, J., Popescu, M., and Sedev, R., "Dynamics of Wetting from and Experimental Point of View," *Annual Review of Materials Research*, Vol. 38, 2008, pp. 23–43. doi:10.1146/annurev.matsci.38.060407.130231

[11] Weislogel, M. M., "Survey of Present and Future Challenges in Low-g Fluids Transport Processes," NASA CR C-74461-N, 2001.

[12] Siegert, C. E., Petrash, D. A., and Otto, E. W., "Time Response of Liquid–Vapor Interface After Entering Weightlessness," NASA TN D-2458, 1964.

[13] Weislogel, M. M., and Ross, H. D., "Surface Settling in Partially Filled Containers upon Step Reduction in Gravity," NASA Lewis Research Center, TM 103641, Cleveland, OH, Nov. 1990.

[14] Weislogel, M., "Fluid Interface Phenomena in a Low-Gravity Environment: Recent Results from Drop Tower Experimentation," *Space Forum*, Vol. 3, Gordon and Breach, Amsterdam, 1998, pp. 59–86.

[15] Michaelis, M., Dreyer, M. E., and Rath, H. J., "Experimental Investigation of the Liquid Interface Reorientation upon Step Reduction in Gravity," *Annals of the New York Academy of Sciences*, Vol. 974, 2002, pp. 246–260. doi:10.1111/j.1749-6632.2002.tb05911.x

[16] Dreyer, M. E., *Free Surface Flows Under Compensated Gravity Conditions, Series: Springer Tracts in Modern Physics*, Vol. 221, Springer–Verlag, New York, 2006.

[17] Hocking, L. M., "Waves Produced by a Vertically Oscillating Plate," *Journal of Fluid Mechanics*, Vol. 179, 1987, pp. 267–281. doi:10.1017/S0022112087001526

[18] Ting, C. L., Perlin, M., "Boundary Conditions in the Vicinity of the Contact Line at a Vertically Oscillating Upright Plate: An Experimental Investigation," *Journal of Fluid Mechanics*, Vol. 295, July 1995, pp. 263–300. doi:10.1017/S0022112095001960

[19] Wölk, G., Dreyer, M., Weislogel, M. M., and Rath, H. J., "Damped Oscillations of a Liquid/Gas Surface upon Step Reduction in Gravity," *Journal of Spacecraft and Rockets*, Vol. 34, No. 1, Jan.–Feb. 1997, pp. 110–117. doi:10.2514/2.3179

[20] Weislogel, M. M., "Spontaneous Steady Capillary Flow in Partially Coated Tubes," *AIChE Journal*, Vol. 43, No. 3, March 1997, pp. 645–654. doi:10.1002/aic.690430310

[21] Tadmor, R., "Line Energy and the Relation Between Advancing, Receding, and Young Contact Angles," *Langmuir*, Vol. 20, No. 18, 2004, pp. 7659–7664. doi:10.1021/la049410h

[22] Jenson, R. M., "Capillary-Driven Corner Flow in Weakly 3-Dimensional Conduits and Contact Line Interface Dynamics in Reduced Gravity Environments," M.S. Thesis, Portland State Univ., Portland, OR, 2008.

I. Boyd
Associate Editor